

Processing, microstructure, and properties of a YAG-based ceramic cutting tool material for titanium alloy machining

Tai-Il Mah*, Hee Dong Lee, Triplicane A. Parthasarathy and Michael K. Cinibulk^a

UES Inc., 4401 Dayton-Xenia Rd., Dayton, OH 45432-1894

^aAir Force Research Laboratory, Materials and Manufacturing Directorate, AFRL/MLLN, Wright-Patterson AFB, OH 45433-7817

A new ceramic composite cutting tool material (YST)⁺, based on a YAG ($Y_3Al_5O_{12}$) matrix, was developed for the improved machining of titanium alloys. Reaction couple studies of the cutting tool material, as well as YAG single crystals, with commercial grade titanium showed the formation of a thin passivating layer of Y_2O_3 next to the composite which is exceptionally resistant to attack by titanium. The YST cutting tools developed in this study are electrically conductive and were easily machined using electro-discharge machining. Microstructural analysis of fully dense YST, using optical, scanning, and transmission electron microscopies, revealed the presence of three distinct constituent phases (YAG, SiC_{w} , and TiC) with no discernible reaction amongst the phases. The average four-point flexural strength of the YST was approximately 700 MPa and the fracture origins were identified as large TiC particles or TiC particle-agglomerates. Analysis of fracture toughness measurements, based on the indentation induced controlled surface flaw/strength technique, showed a pronounced rising R-curve behavior of YST. The SEM analyses showed clear evidence of SiC whisker pullouts and bridging, which support the rising R-curve behavior of YST. Preliminary machining experiments using the YST cutting tool (not yet optimized) on Ti-6Al-4V alloy showed similar machining characteristics as conventional cutting tool materials (e.g., cemented carbides). It is suggested that process optimization will yield significantly improved cutting tools for titanium machining.

Key words: YAG based new ceramic composite, cutting tool, titanium alloy.

Introduction

Among alloys of industrial interest, titanium alloys represent one of the most difficult materials to machine. In fact, machining of titanium alloys has become a major limitation in aerospace manufacturing because, unlike steels and nickel-based alloys, titanium cannot be machined satisfactorily at high cutting speeds (>200 m/s) even with advanced ceramic cutting tools [1-3]. Titanium alloys have low thermal conductivities and high work-hardening characteristics, which lead to rapidly rising cutting temperatures (up to 1100 °C) [3] at even low cutting speeds (<50 m/minute). Due to the high machining temperatures and the high chemical reactivity of titanium with most currently available ceramic tool materials, titanium alloys are still machined with cemented carbide tools at speeds only incrementally higher than those employed when the first titanium alloys became available [3]. As a result, production times are long and costly.

While ceramic cutting tools have found increased application in the machining of materials that are difficult to cut, such as nickel-based superalloys, they have not replaced cemented carbides due to their high

reactivity with titanium. Also, only limited success has been achieved in using coatings to minimize reactivity and diffusion of carbon from the conventional tungsten carbide tools to the titanium workpiece [3, 4]. It is clear that the requirements for a ceramic cutting tool for the machining of titanium alloys at high speeds are not satisfied with currently available cutting tools. A new cutting tool material that displays the attractive properties of the current state-of-the-art ceramic cutting tools while being chemically compatible with titanium would dramatically increase cutting rates, improve surface finish, and provide extended lifetimes of the cutting tool itself.

There are three primary requirements for a material that is to be used as a cutting tool for titanium. First, the material must have sufficient hardness at the elevated temperatures (~ 1000 °C) at which titanium alloys are machined. This may dictate that the material must have not only high resistance to fast-fracture, but also resistance to creep-rupture. Second, the fracture toughness must be high enough to withstand the stresses generated by machining titanium alloys at high cutting speeds. Reinforcing second phases are likely to be needed to increase fracture toughness. Third, a material that is stable with highly reactive titanium at the high temperatures generated during machining is required.

Kramer *et al.* [5] performed a preliminary thermod-

*Corresponding author:
Tel : +1-937-255-9829
Fax: +1-937-656-7292
E-mail: Taiil.Mah@wpafb.af.mil

ynamics-based analysis to identify potential tool materials that are compatible with titanium. A number of compounds, particularly rare-earth oxides, were found to be chemically compatible with Ti. While simple oxides of the rare-earth elements were considered, multicomponent rare-earth-containing compounds containing multiple cations were not. Therefore, a new ceramic composite with increased stability for the machining of titanium alloys was formulated. This new cutting tool composition replaces the alumina matrix in conventional ceramic cutting tools with yttrium-aluminum garnet (YAG), which has similar mechanical properties to alumina, yet is thermodynamically compatible with titanium. YAG is being considered for high-temperature structural applications for its superior high-temperature mechanical properties; for example, it is the most creep resistant oxide known [6-8]. Preliminary results on the composite fabrication, chemical compatibility of the composite constituents and chemical compatibility of the composite with titanium, the mechanical properties, microstructural characterization and electrodischarge machineability (EDM) of the composites are described in this publication.

Experimental Procedures

Composite Fabrication

The nominal composition of the YST cutting tool was 43% YAG, 33% SiC whiskers, and 24% TiC by volume. The as-received YAG powder (Sasol North America, Inc., Ceralox Division, Tucson, AZ) contained a small amount (~5%) of an intermediate reaction product, YAlO_3 , and residual yttria and alumina. In order to reduce the particle size of the as-received YAG powder (~5.5 μm), the powder was ball-milled for 100 hr using high-purity alumina balls (99.5%) in a water medium. The average particle size was reduced to 1.7 μm . The TiC powder was used in both the as-received condition (YST/UES-1) and as fines separated by sedimentation (YST/UES-2, 3, 4). The milled YAG powder and TiC powder were wet milled together prior to blending with the SiC whiskers (early 80s vintage of ARCO through the courtesy of Dr. Robert Ruh, AFRL). The milled powder was dried and calcined at 600 °C to remove organic contaminants obtained during milling. Hot-pressing of the composites (~2.54 cm diameter) was carried out in vacuum (~0.2 torr) at ~1800 °C/25 MPa/30 minutes. The YST used for the R-curve study was processed by ICT (Industrial Ceramics Technology, Inc., Ann Arbor, MI) based upon our specifications. The SiC whiskers used by ICT were from Tokai Carbon Co. Ltd., Tokyo, Japan, and the same YAG powder (Ceralox). The constituent materials were mixed using ICT proprietary processing and were then vacuum hot-pressed into billets of size 12.7 cm in diameter and ~6.5 mm thick. The nominal composition of the YST was the same as the ones used for strength tests. The two YST (#102 and #103) billets used for R-curve

study were 97.7 and 98.1% of theoretical density, respectively.

Thermodynamic Analysis and Reaction Couples: Thermochemical Stability

Thermodynamic calculations were performed to determine the reactivity of YAG with the workpiece of interest, titanium/titanium aluminide and with the various components of the cutting tool material. The free energies of reactions were computed for YAG and compared with those computed for alumina, the competing matrix material for the cutting tool. The required data were obtained from published data by Chase *et al.*, Turkdogan, and Kubaschewski *et al.* [9-11].

The components selected for the studies were (1) Ti, (2) SiC, (3) TiB_2 , and (4) TiN. For reactions with titanium aluminide, the free energies of formation with pure titanium were converted to equilibrium Ti activities (assuming the activity of all other components to be unity) and then compared with the calculated equilibrium activity of Ti in TiAl.

To study the kinetics of the reaction of titanium with YAG, a reaction couple was prepared. The face of a single crystal YAG coupon (~1 cm \times 1 cm) was polished to a 1- μm finish using diamond paste. Commercial purity (CP) titanium foil (~125 μm thick) was sandwiched between the polished faces of two coupons and held together with platinum wire. The reaction couple was placed in a quartz-glass envelope, evacuated, backfilled with high-purity argon, and sealed. The encapsulated reaction couple was heated for 2 hr at 800° to 1200 °C. For comparison, CP titanium reaction couples with YAG- and alumina-containing cutting tool materials (YST and AST) were made in the same manner.

Mechanical Testing : Strength and Fracture Toughness – Strength

Bend bars were cut from the hot-pressed billet so that the tensile surfaces of the test bars were parallel to the hot-pressing direction and the crack propagated perpendicular to the hot-pressing direction. The tensile surface of each bar was polished with diamond paste to a 1- μm finish and the edges were chamfered with a diamond wheel.

– R-Curve

From each billet (YST-#102 and #103), 16 bend bars (~3.175 \times 6.35 \times 50 mm) having the tensile surface parallel and 16 having the tensile surface perpendicular to the hot-pressing direction were machined using a diamond saw. The tensile surfaces of the bend bars were ground with a 600 grit diamond grinding/polishing wheel and the final polish was done using a 6 μm diamond disc. Sample edges were beveled. R-curve measurements were carried out using an indentation-induced controlled surface flaw technique. A Vickers indentation was placed at the middle of the tensile surface of the bend bar. The indentation loads used were 1, 2, 5, 10, and 20 kg; 3 tests were performed for

each load, for each group of specimens (samples #102 and #103, parallel and perpendicular to hot-pressing direction). Optical microscopy was used to measure the surface projection of the radial cracks. The half-length of the surface crack was taken as the radii of the indentation induced crack. Both strength and R-curve tests were performed using a four-point-bending configuration with an inner span of 9.525 mm and an outer span of 38.1 mm for strength and 19.01 mm and 38.1 mm for R-curve, respectively. The cross-head speed used was 0.127 mm/minute.

Microstructural and Fractographic Analyses

The microstructures of the composites were examined both parallel and perpendicular to the hot-pressing direction using optical and scanning electron microscopy (SEM). Selected samples were examined using TEM to study any possible reaction amongst the constituents. The fracture surfaces of the test bars were examined using SEM to determine the fracture origin and pulled out whiskers and corresponding holes. Indentation induced cracks were examined using SEM to observe crack bridging by SiC whiskers.

Preliminary Titanium Machining

A limited number of composite samples were machined into tool inserts (CNG-432) and a machining experiment was carried out to determine the preliminary machining characteristics of the composite.

Results and Discussion

Thermodynamic Compatibility of constituents and Titanium Alloys

The reactions considered for the calculations on reactivity with titanium are as follows. (YAG represents $Y_3Al_5O_{12}$)

- 1) $Ti + Al \rightarrow TiAl$
- 2) $Ti + (2/15) YAG \rightarrow TiO + (3/15) Y_2O_3 + (1/3) Al_2O_3$
- 3) $Ti + (1/3) Al_2O_3 \rightarrow TiO + (2/3) Al$
- 4) $Ti + (2/3) Al_2O_3 \rightarrow TiO_2 + (4/3) Al$
- 5) $Ti + (3/8) SiC \rightarrow (1/8) Ti_5Si_3 + (3/8) TiC$
- 6) $Ti + (3/8) SiO_2 \rightarrow (1/8) Ti_5Si_3 + (3/8) TiO_2$

Reactions to form TiO were always more favorable, and hence used for comparisons. Reaction (6) was included to determine the reactivity of SiC in the presence of air at temperature. The free energies of the reactions were used to calculate the equilibrium titanium activity, assuming all other products/reactants had an activity of unity. The calculations showed that both SiC and silica (oxidation product of SiC) are predicted to react with TiAl. The calculated activity of Ti in equilibrium for various reactions is shown in Fig. 1. YAG is superior to alumina, although the activity of Ti in TiAl is below that for reaction with both alumina

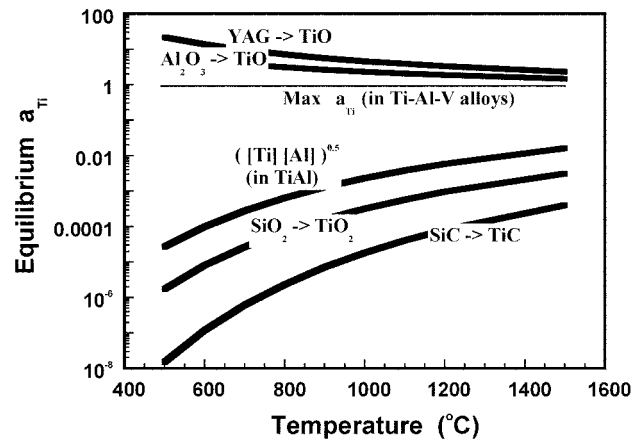


Fig. 1. Calculated activity of Ti in equilibrium for various reactions showing the relative stability of YAG and alumina against TiAl. YAG is seen to have a better stability against reaction with titanium than alumina.

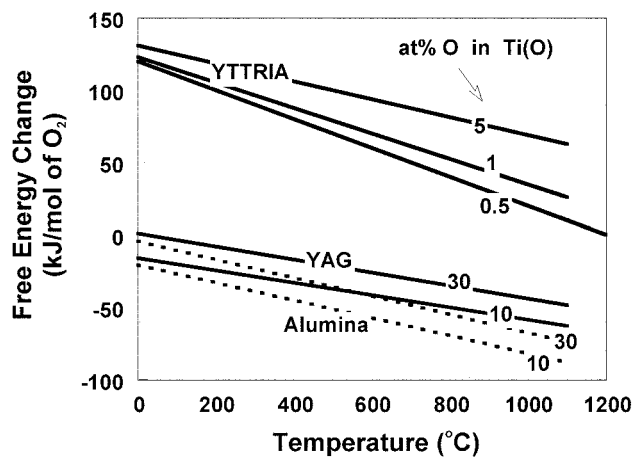


Fig. 2. Calculated thermodynamic free energies of reactions involving reaction by dissolution of oxygen in Titanium. Both YAG and Alumina are predicted to react while yttria is predicted to be stable.

and YAG. The tendency for reaction increases with temperature in both cases. Since it is known that alumina reacts with titanium, it is possible that one needs to calculate the thermodynamics of oxygen dissolution in titanium (thermodynamic data for sub-oxides of Ti ($TiO_{0.5}$) are available but they were found to be even less favorable). The free energy change was calculated as a function of atomic percent oxygen dissolved in titanium using the data from Kubaschewski *et al.* [11] The reactivity of YAG, alumina and yttria were calculated and compared (Fig. 2). The following reactions were considered.

- 1) $(1-X)/X Ti + (4/15) YAG \rightarrow (1-X)/X Ti(O) + (2/5) Y_2O_3 + (4/3) Al$
- 2) $(1-X)/X Ti + (2/3) Al_2O_3 \rightarrow (1-X)/X Ti(O) + (4/3) Al$
- 3) $(1-X)/X Ti + (2/3) Y_2O_3 \rightarrow (1-X)/X Ti(O) + (4/3) Y$

X is the atomic fraction of oxygen dissolved in titanium. The results were compared at $X=0.1$ for alumina and YAG and at $X = 0.01, 0.05, 0.1$ for Y_2O_3 . The free energy was always negative for alumina and YAG. For yttria, the free energy was positive below a critical temperature. This temperature was close to $1100\text{ }^\circ\text{C}$ for 0.4 at% dissolved oxygen in Ti, and lower for lower oxygen concentrations. Thus it appears that YAG is not sufficiently better than alumina; however if YAG is reduced to yttria and if yttria physically separates YAG from Ti, further reaction might be suppressed provided an atomic concentration of 0.4% is allowed to accumulate in the titanium.

The other objective of the work was to estimate the reactivity of YAG with other constituents of the cutting tool (listed in the experimental section) and compare the results with those for alumina. These calculations are useful for predicting the stability of the constituents during both processing, as well as during use. The calculations showed that the only compound that is predicted to react with YAG is silica, the oxidation product of SiC. The reactivity of alumina was calculated using the appropriate reaction equations. The reactivity was found to be worse than YAG in all cases; this is not surprising since all the reactions are based on decomposing YAG followed by a reaction with alumina.

Reaction Couples and Kinetics

Thermodynamic calculations were verified experimentally by characterizing the interface between reaction couples of the composites (YST and AST) and commercially pure titanium foil heated in argon for 2 h at temperatures of 800° to $1200\text{ }^\circ\text{C}$.

In the case of single-crystal YAG and Ti, YAG was found to partially decompose to Y_2O_3 , resulting in a thin, $1\text{-}\mu\text{m}$ thick layer of Y_2O_3 (Fig. 3). No Y was detected in the Ti foil. For the YST composite (earlier hot-pressed specimen from ICT having $\sim 5\%$ porosity), YAG was found to decompose, resulting in a layer of

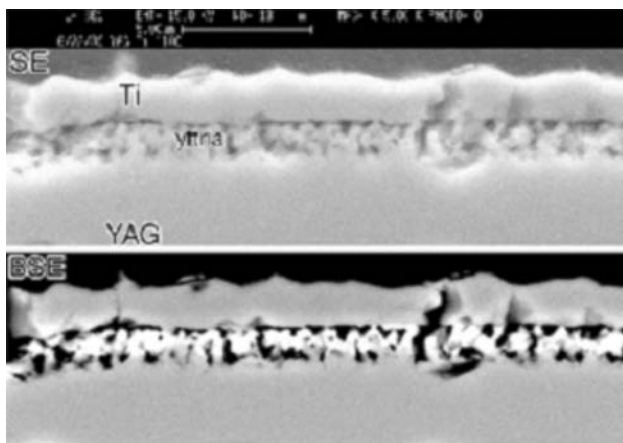


Fig. 3. SEM images of the single-crystal YAG-Ti reaction couple after heating at $1100\text{ }^\circ\text{C}/2\text{ hr}$. The bright phase in the BSE image is the Y_2O_3 reaction product.

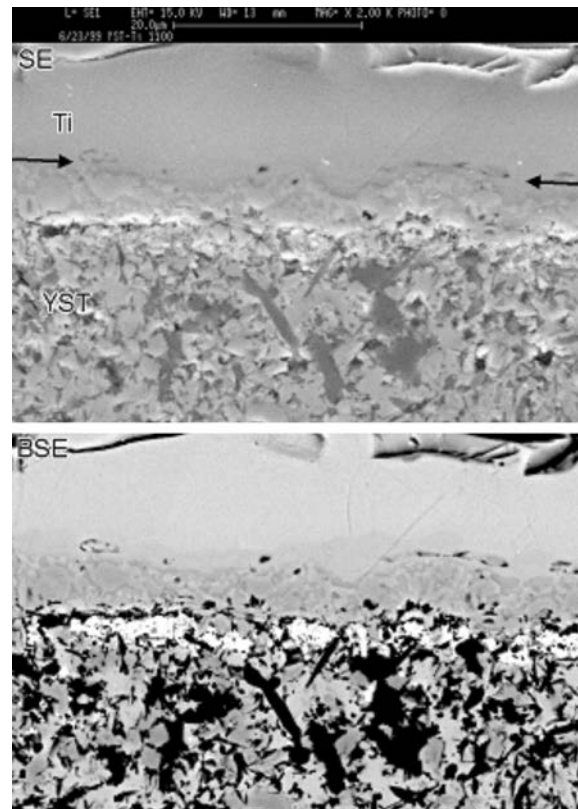


Fig. 4. Secondary-electron and backscattered-electron images of the YST-Ti interface after heating at $1100\text{ }^\circ\text{C}$. Arrows indicate position of original interface. In BSE image lightest phase next to YST is Y_2O_3 reaction product. Mottled layer above Y_2O_3 is Ti (rich in Si) and TiC.

Y_2O_3 next to the composite. At the highest temperature of $1200\text{ }^\circ\text{C}/2\text{hr}$, the reaction affected only the top $15\text{ }\mu\text{m}$ of the YST composite coupon, but at $1100\text{ }^\circ\text{C}/2\text{ h}$, only the top $10\text{-}\mu\text{m}$ of the composite was affected (Fig. 4). No Y was found in the Ti. The thickness of the decomposition product was $3\text{ }\mu\text{m}$ (Fig. 4), compared to $1\text{ }\mu\text{m}$ for that found in the YAG single-crystal at the same temperature. The high porosity ($\sim 95\%$ of theoretical density) of the unoptimized YST material is likely the cause for the greater Ti reactivity. Also, it is clear that the presence of SiC increases the total depth to which the reaction proceeds in YST, when compared to that of YAG alone.

Figure 5 contains EDS elemental maps of the YST-Ti interface heated to $1100\text{ }^\circ\text{C}$ for 2 h. There was a thin Y-rich region between the composite and metal, devoid of any other cations. Al and Si are present in significant quantities in the titanium in either solid solution, or in the case of Si, as a distinct phase, as is TiC. As the temperature is increased, the thickness of the reaction zone is increased. The titanium seems to enter the composite by dissolving aluminum and SiC, leaving behind a TiC skeleton. As YAG decomposes, a thin layer of Y_2O_3 is left at the advancing Ti-composite interface. While yttria is not compatible with alumina, the yttrium-containing aluminates [12] that normally

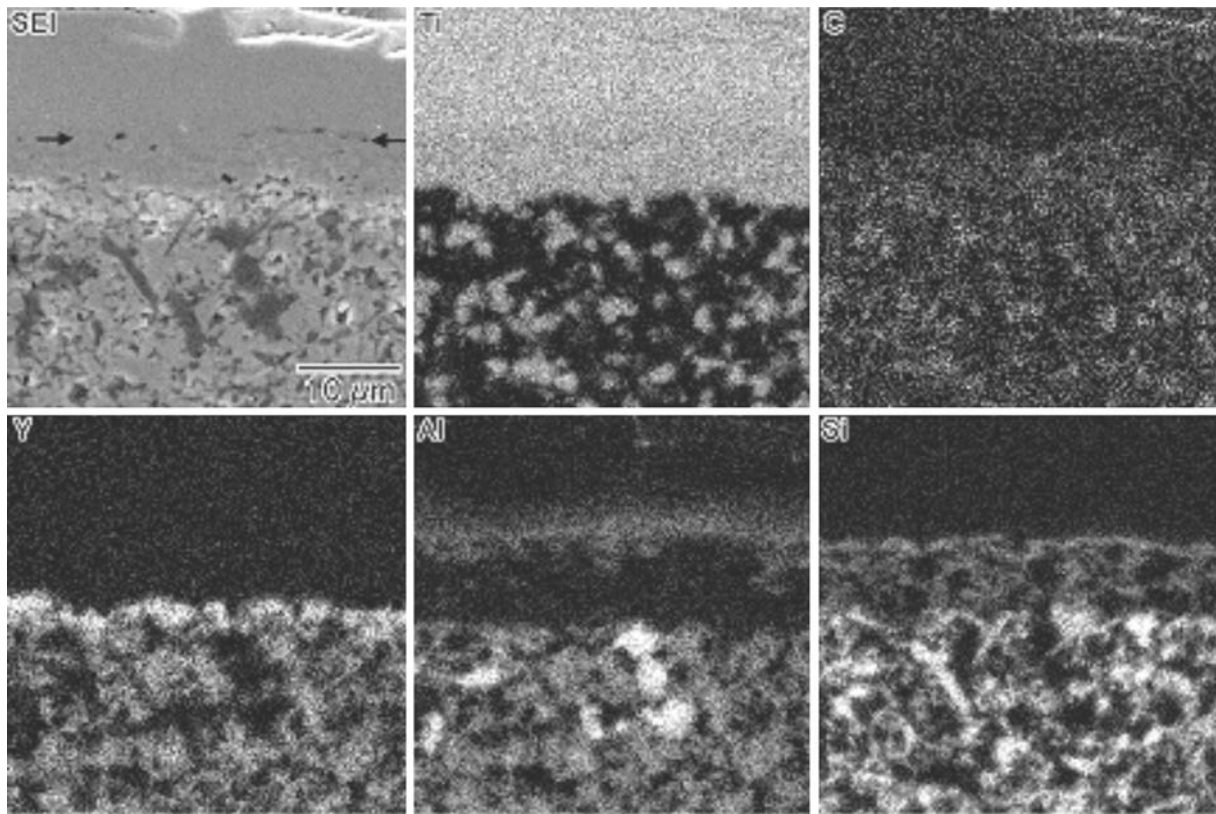


Fig. 5. Secondary-electron image and EDS elemental maps of the central region of interfacial area shown in Fig. 4.

would be expected to form do not. The affinity of titanium for aluminum and oxygen is so high that only Y_2O_3 , and perhaps elemental Y, is left behind. No Y is found in the titanium metal, either as a distinct phase or in solution. Since Y_2O_3 forms as a layer between the advancing Ti and the remaining composite, and no Y is observed in the Ti itself, the Y_2O_3 decomposition product seems to be acting as an effective diffusion barrier to slow the reaction. This indicates that while YAG is indeed quite resistant to reaction with Ti, the presence of SiC in the composite results in an increased reaction. It appears that Y_2O_3 acts as a diffusion barrier between the remaining unreacted composite and the advancing titanium. Thermodynamic calculations show that Y_2O_3 is exceptionally resistant to attack by titanium (Fig. 2). At 1200 °C, the equilibrium (with Y_2O_3) concentration of oxygen dissolved in titanium is calculated to be only 0.5 at%. In contrast, Ti can completely reduce Al_2O_3 by dissolving oxygen as solid solution in Ti. The alumina-based AST composite tool showed a greater reaction product thickness than the YST material. Clearly, the affinity of Ti for Al is high and it appears that Al_2O_3 decomposes and Al goes into solution much faster than the decomposition of YAG.

Microstructures of YST Composite Cutting Tool

The optical micrographs of YST/UES-1 to 4 are shown in Fig. 6. The variations in TiC particle size

(light phase) are easily discernible. As will be discussed later, the TiC particle size in the YST composites affects the mechanical properties as well as the EDM machinability. The YST/UES-1 sample shows the presence of a wide range of TiC particle sizes (up to 70–80 μm). This sample was extremely difficult, if not impossible, to EDM machine. Through sedimentation classification, the particle size of the TiC was considerably reduced, as shown in the YST/UES-2 sample. This composite was readily EDM machined. Further refinement of the TiC particles before hot-pressing showed a better distribution of TiC in the composite (YST/UES-3). The YST/UES-4 sample, fabricated using the YST/UES-3 powder batch, was ~5 cm in diameter and the machining tool inserts (CNG-432) were machined from this billet. The samples were also examined parallel to the hot-pressing direction and, surprisingly, no obvious difference from Fig. 6 (perpendicular to hot-pressing direction) was observed.

SEM micrograph (Fig. 7) of YST/UES-3 shows details of the phase distribution and also the preservation of SiC whiskers during processing. X-ray diffraction analyses (XRD) of YST were carried out before and after the composite hot-pressing. The XRD patterns of both were identical, which suggests phase compatibility during hot-pressing. A TEM micrograph of YST/UES-3 is shown in Fig. 8. Three constituent phases are clearly shown and no reaction amongst

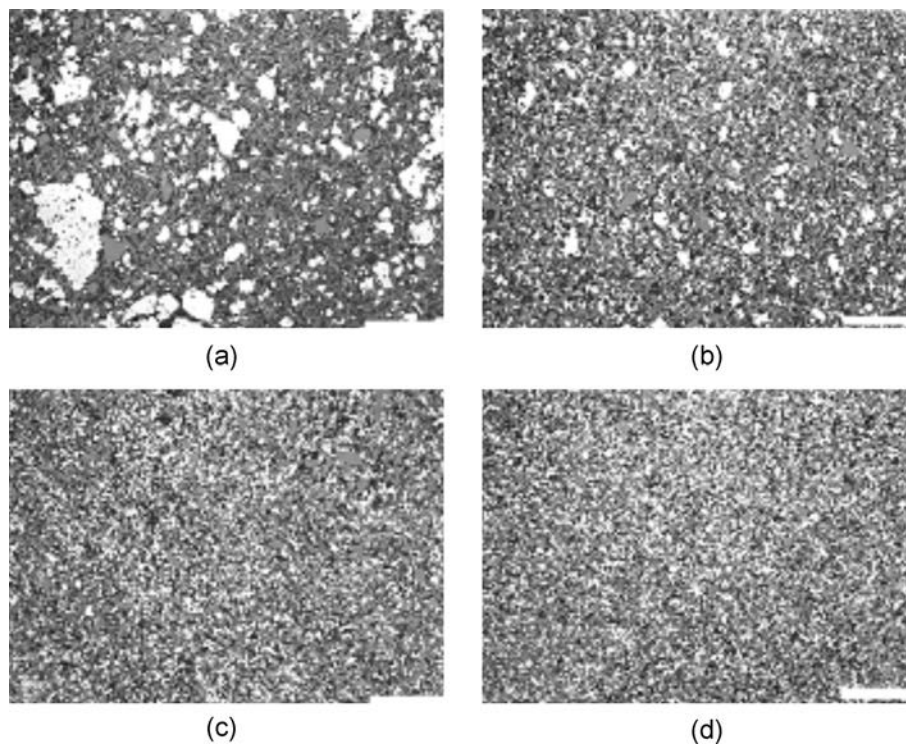


Fig. 6. Optical Micrographs of YST/UES-1 to 4 (a to d) Perpendicular to Hot-Pressing Direction (bar = 10 μm).

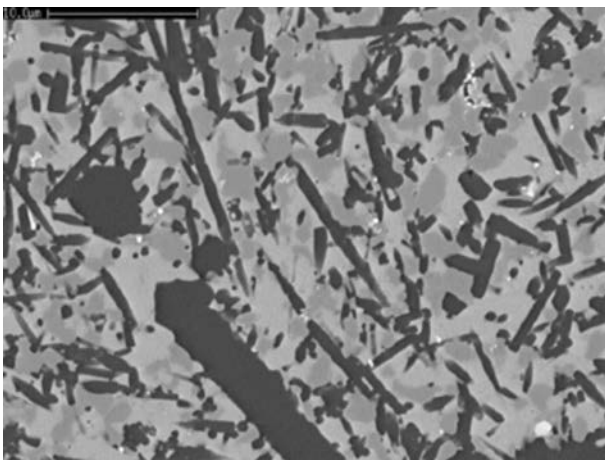


Fig. 7. SEM (SEI) Photomicrograph of YST/UES-3 taken from perpendicular to the hot-pressing direction showing three distinct constituent phases (light: YAG, grey: TiC, and dark: SiC whiskers). SiC whiskers vary in sizes and aspect ratio.

these phases is apparent. An abundance of very fine (< 100 nm) TiC particles along with large (> 1 μm) TiC particles were observed. Some of the small TiC particles were embedded in the YAG, which suggests entrapment of TiC particles during sintering of YAG. The YAG phase appears to fill the interstices and conformed to accommodate the TiC and SiC phases. At the hot-pressing temperature (~1800 $^{\circ}\text{C}$), both YAG and TiC should be quite ductile, promote complete densification of the cutting tool composite.



Fig. 8. TEM Micrograph of YST/UES-3 showing small entrapped TiC particles in YAG.

Mechanical Properties of YST Composite Cutting Tool

The flexural strengths of YST/UES samples are shown in Fig. 9. About a 35% improvement in strength was observed for the YST/UES-3 (692 MPa) compared to the YST/UES-1 (516 MPa). The YST/UES-2 sample showed an intermediate strength between 1 and 3. Since only the TiC particle size was varied between these sets of samples, the starting TiC particle size refinement results in the improvement in strength. SEM fractographic analyses confirmed this conclusion. The fracture origin for the YST/UES-1 samples was

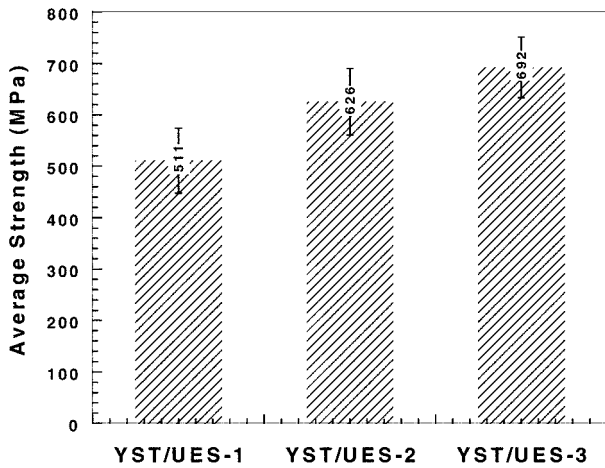


Fig. 9. Four-point-bend strength of YST materials. The numbers in the plot are the average values.

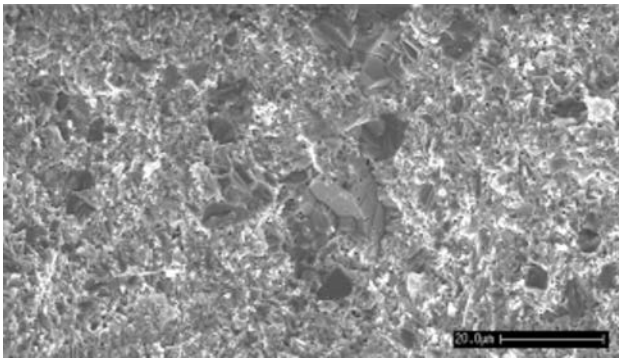


Fig. 10. SEM fractograph of the YST/UES-1 sample showing agglomeration of TiC particles near tensile surface (top) of the bend bar ($\sigma = 493$ MPa).

identified as an agglomerate of large TiC particles (Fig. 10). This observation is in accordance with the presence of large TiC particles in the sample (Fig. 6). The fracture initiating flaw in YST/UES-3 also appeared to be a large ($\sim 10 \mu\text{m}$) TiC particle (Fig. 11). The mating piece of the fractured sample did not reveal any unusual features near the fracture origin.

Since the publication by Wei and Becher [13] regarding attractive mechanical properties of SiC whisker reinforced alumina, various organizations reported more detailed analysis of this type of material [14-30]. In this study the R-curve analysis followed the technique described by Krause *et al.* [18, 22], and Cook and Clark [19] using the same nomenclature,

$$K_R = k(\Delta a)^m$$

where K_R is fracture resistance of the material, Δa is crack extension, and k and m are constant. Through measuring the fracture strength (S) of the bend bars with indentation flaw with various load (P), $\log S$ vs. $\log P$ plot having relations of $S = \alpha P^{-\beta}$ can be generated, where the exponent b is defined by $m = (1 - 3\beta)/(2 +$

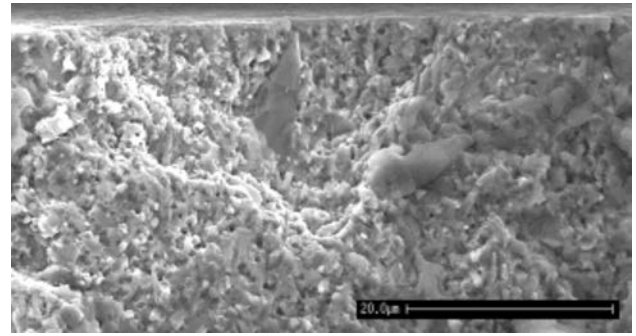


Fig. 11. SEM fractograph of the YST/UES-3 sample showing the presence of large ($\sim 10 \mu\text{m}$) TiC particle near tensile surface (top) of the bend bar ($\sigma = 711$ MPa).

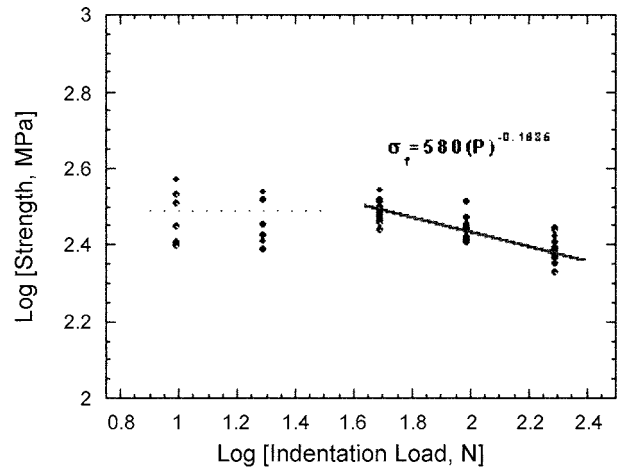


Fig. 12. Flexural strength of YST as a function of Vicker's indentation load. The solid line is a least-squares fit for the data.

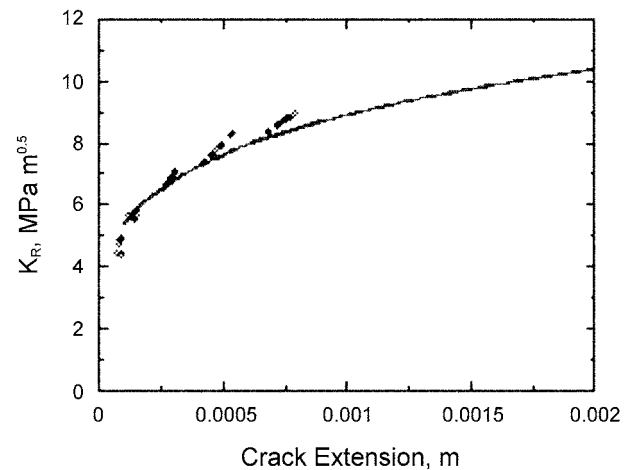


Fig. 13. Fracture resistance (K_R) versus crack extension (Δa) for YST showing rising R-curve behavior.

$2\beta)$ and the coefficient α is defined by $k = Y\alpha(\beta\gamma)^{-\beta} (1+\beta)^{(1+\beta)}$, where Y is a configuration coefficient constant and γ is defined as $\gamma = P/(a_i)^{2/(3+2m)}$, where a_i is the indentation-induced initial crack depth.

The coefficients β and $\log(\alpha)$ can be evaluated by a linear least-square fit from the plot shown in Fig. 12.

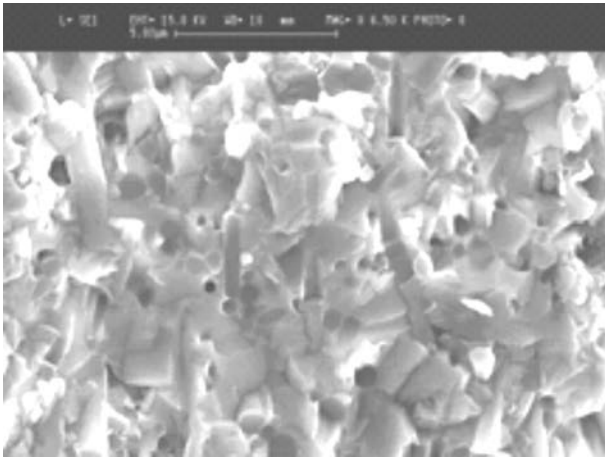


Fig. 14. SEM fractograph of YST showing SiC_w pull-outs and corresponding holes/troughs at the wake of crack.

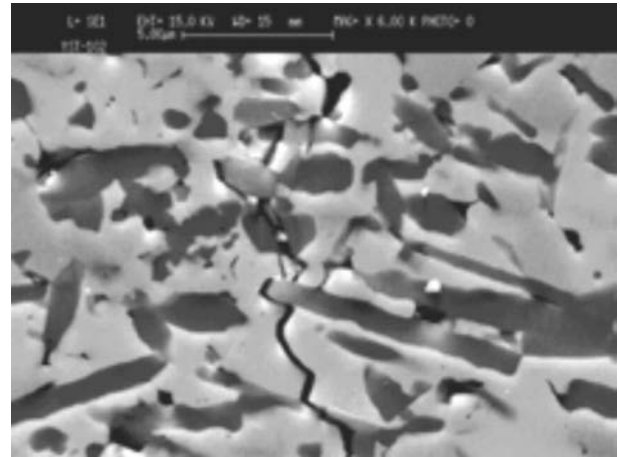


Fig. 15. SEM micrograph of YST surface showing crack bridging by SiC_w (dark phase) along Vicker's indentation crack path (top to bottom).

The slope of the plot, $d \log (S)/d \log (P) = -\beta$, is -0.1635 and is about half of the value $1/3$, which is fracture toughness independent of crack extension. Figure 13 shows the calculated fracture resistance of the YST increasing as a function of crack extension. The K_R of the YST increased from ~ 4.5 to ~ 9 MPa \sqrt{m} with a corresponding increase in Δa from ~ 100 to ~ 800 μm . The increase in K_R with increasing Δa indicates the crack wake toughening is operating. The evidence of whisker pullouts can be seen clearly on the fracture surface of YST in Fig. 14. SiC whisker bridging is also evident in Fig. 15, which is an SEM micrograph of a crack produced from a Vickers indentation. Similar type of plots of Figs. 14 and 15 for each set of samples (#102 and #103) and testing orientations (parallel and perpendicular to hot-pressing direction) were made to study the reproducibility and preferred microstructural differences. Obvious differences were not detected and the Figs. 14 and 15 were constructed including all the test data.

Machining of Titanium Alloys

The major advantage of the YST cutting tool over the conventional ceramic cutting tool is that the YST can be machined using electrodischarge machining (EDM). The EDM machinability of YST is clearly demonstrated in Fig. 16, where 5 and 12 mm discs were wire EDMed out. A SEM photomicrograph of the cut surface of YST after EDM is also shown in Fig. 16. The SEM micrograph was taken at the edge of the YST specimen to show both the as-ground (left) and the EDM cut (right) surfaces. The roughness of the EDM cut surface of YST is comparable to a typical metal cut surface. The EDM machining rate was similar to Mo or W machining rates with a similar thickness.

The machining tool inserts (CNG432) were machined from YST/UES-4. The workpiece used were Ti-6Al-4V and Inconel 718. Thus far the test results are only qualitative. With the CNG432 geometry, the YST faired similar to other commercial cutting tools (as judged by machinist). It was noted that the YST cutting

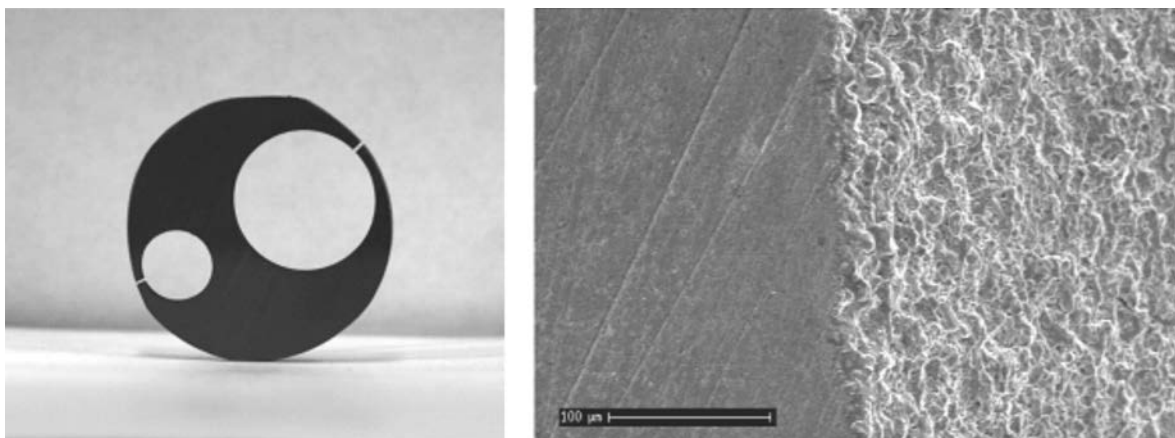


Fig. 16. Optical (machined out two discs of 5 and 12 mm in diameter) and SEM (left = as-ground billet surface and right = EDM machine cut surface) Photomicrograph of YST specimen after wire EDM machining.

tool showed a great potential since it has not been optimized yet. New cutting tool inserts (from pseudo-optimized processing) are being machined and the machining experiment results will be reported in later publication.

Summary and Conclusion

A new ceramic composite cutting tool material (YST), based on YAG matrix, was developed for the improved machining of titanium alloys. The reaction couple study of the cutting tool material as well as YAG single crystal with commercial grade titanium showed YAG is found to decompose, resulting in a thin layer of Y_2O_3 next to the composite which is exceptionally resistant to attack by titanium. The YST cutting tools, developed in this study, are electrically conductive and were easily machined using electro-discharge machining. The microstructural analysis of fully dense YST with optical, scanning, and transmission electron microscopies revealed the presence of three distinct constituent phases (YAG, SiC_w , and TiC) and no discernible reaction amongst three phases. The average four-point flexural strength of the YST with small TiC particles was approximately 700 MPa and the fracture origins were identified as large TiC particles or TiC particle agglomerates. R-curve analysis, based on the indentation induced controlled surface flaw/strength technique showed rising R-curve behavior of YST. The SEM analysis showed clear evidences of SiC whisker pullouts and bridging, which indicate the crack wake toughening is operating in YST. Preliminary machining experiments using YST cutting tool (not yet optimized) on Ti-6Al-4V alloy showed similar machining characteristics as conventional cutting tool materials (e.g., cemented carbides) and potential for further improvement.

Acknowledgment

We appreciate technical support from Mr. Charles Cooke and Mr. Marlin Cook. We also acknowledge Ms. Kristin Keller for SEM and Dr. Pavel Mogilevsky for TEM analyses.

References

1. N. Narutake and A. Murakoshi, *Annals CIRP* 32[1] (1983) 52-57.
2. J. Kertesz, R.J. Pryor, D.W. Richerson, and R.A. Cutler, *J. Met.* 40 (1988) 50-51.
3. E.O. Ezugwu and Z.M. Wang, *J. Mater. Process. Technol.* 68 (1997) 262-274.
4. P.D. Hartung and B.M. Kramer, *Annals CIRP* 31[1] (1982) 75-79.
5. B.M. Kramer, D. Viens, and S. Chin, *Annals CIRP* 42[1] (1993) 111-114.
6. G.S. Corman, *J. Mater. Sci. Lett.* 12 (1993) 379-382.
7. T.A. Parthasarathy, T. Mah, and K. Keller, *J. Am. Ceram. Soc.* 75[7] (1992) 1756-1759.
8. S. Karato, Z. Wang, and K. Fujino, *J. Mater. Sci.* 29 (1994) 6458-6462.
9. M.W. Chase, C.A. Davies, J.R. Downey, D.J. Frurip, R.A. McDonald, A.N. Syverud, *JANAF Thermochemical Tables*, 3rd edition, *Jl of Phys. And Chem. Ref. Data*, 14 (1985).
10. E.T. Turkdogan, "Physical Chemistry of High Temperature Technology", Academic Press, NY (1980).
11. O. Kubaschewski, C.B. Alcock, P.J. Spencer, "Materials Thermochemistry", 6th edn, Pergamon Press, NY (1993).
12. T. Mah, K.A. Keller, S. Sambasivan, and R.J. Kerans, *J. Am. Ceram. Soc.* 80[4] (1997) 874-878.
13. G.C. Wei and P.F. Becher, *Am. Ceram. Soc. Bull.* 64[2] (1985) 298-304.
14. J. Homeny, W.L. Vaughn, and M.K. Ferber, *Am. Ceram. Soc. Bull.* 65[2] (1986) 333-338.
15. M.G. Jenkins, A.S. Kobayashi, K.W. White, and R.C. Bradt, *J. Am. Ceram. Soc.* 70[6] (1987) 393-395.
16. P. Angelini and P.F. Becher, *Proceedings of the Electron Microscopy Society of America*. Edited by G.W. Bailey. San Francisco Press, San Francisco, CA (1987) p. 148-149.
17. M. Ruhle, B.H. Dalglish, and A.G. Evans, *Scr. Metall.* 21 (1987) 681-686.
18. R.F. Krause, Jr., *J. Am. Ceram. Soc.* 71[5] (1988) 338-343.
19. R.F. Cook and D.R. Clark, *Acta. Metall.* 36[3] (1988) 555-562.
20. P.F. Becher, C.H. Hsueh, P. Angelini, and T.N. Tiegs, *J. Am. Ceram. Soc.* 71[12] (1988) 1050-1061.
21. G.H. Campbell, M. Ruhle, B.J. Dalgeleish, and A.G. Evans, *J. Am. Ceram. Soc.* 73[3] (1990) 521-530.
22. F. Krause, Jr., E.R. Fuller, Jr., and J.F. Rhodes, *J. Am. Ceram. Soc.* 73[3] (1990) 559-566.
23. J. Homeny and W.L. Vaughn, *J. Am. Ceram. Soc.* 73[7] (1990) 2060-2062.
24. P.F. Becher, *J. Am. Ceram. Soc.* 74[2] (1991) 255-269.
25. P.F. Becher, E.R. Fuller, Jr., and P. Angelini, *J. Am. Ceram. Soc.* 74[9] (1991) 2131-2135.
26. E. Yasuda, T. Akatsu, and Y. Tanabe, *J. Ceram. Soc. Jpn.* 99 (1991) 51-57.
27. T. Akatsu, Y. Tanabe, S. Matsuura, M. Yamada, H. Ishii, M. Munakata, and E. Yasuda, *J. Ceram. Soc. Jpn.* 99 (1991) 416-418.
28. P.F. Becher, C.H. Hsueh, H.T. Lin, K.B. Alexander, T.N. Tiegs, W.H. Warwick, and S.B. Waters, *Ceramic Transactions Vol. 46, Advances in Ceramic-Matrix Composites II*. Edited by J.P. Singh and N.P. Bansal. American Ceramic Society, Westerville, OH (1995) p. 237-261.
29. P.F. Becher, C.H. Hsueh, K.B. Alexander, and E.Y. Sun, *J. Am. Ceram. Soc.* 79[2] (1996) 298-304.
30. T. Akatsu, M. Suzuki, Y. Tanabe, and E. Yasuda, *J. Mater. Res.* 16[7] (2001) 1919-1927.